JACS
JOURNAL OF THE AMERICAN CHEMICAL SOCIETY

ARTICLE

pubs.acs.org/JACS

P-Type Nitrogen-Doped ZnO Nanoparticles Stable under Ambient Conditions

Benoit Chavillon,[†] Laurent Cario,[*,†] Adèle Renaud,[†] Franck Tessier,[§] François Cheviré,[§] Mohammed Boujtita,[‡] Yann Pellegrin,[‡] Errol Blart,[‡] Amanda Smeigh,[∥] Leif Hammarström,[∥] Fabrice Odobel,[‡] and Stéphane Jobic[*,†]

[†]Institut des Matériaux Jean Rouxel (IMN), Université de Nantes, CNRS, UMR6502, 2 rue de la Houssinière, 44322 Nantes cedex 3, France

[‡]CEISAM, Université de Nantes, CNRS, UMR6230, 2 rue de la Houssinière, 44322 Nantes cedex 3, France

[§]UMR CNRS 6226 "Sciences Chimiques de Rennes", équipe Verres et Céramiques, Université de Rennes 1, 35042 Rennes cedex, France

[∥]Department of Photochemistry and Molecular Science, Uppsala University, P.O. Box 523, 75120 Uppsala, Sweden

Supporting Information

ABSTRACT: Zinc oxide is considered as a very promising material for optoelectronics. However, to date, the difficulty in producing stable p-type ZnO is a bottleneck, which hinders the advent of ZnO-based devices. In that context, nitrogen-doped zinc oxide receives much attention. However, numerous reviews report the controversial character of p-type conductivity in N-doped ZnO, and recent theoretical contributions explain that N-doping alone cannot lead to p-typeness in Zn-rich ZnO. We report here that the ammonolysis at low temperature of ZnO_2 yields pure wurtzite-type N-doped ZnO nanoparticles with an extraordinarily large amount of Zn vacancies (up to 20%). Electrochemical and transient spectroscopy studies demonstrate that these Zn-poor nanoparticles exhibit a p-type conductivity that is stable over more than 2 years under ambient conditions.

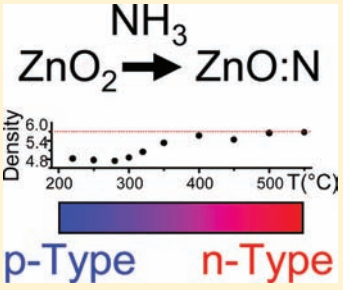

INTRODUCTION

Zinc oxide is considered a very promising material for optoelectronic devices.[1−4] Indeed, in the particular case of the next generation of inorganic light-emitting diodes and lasers, for instance,[5] ZnO appears as a potential substitute for GaN and its derivatives whose production remains costly and polluting. Unfortunately, the advent of such an innovative technology suffers from the lack of easily obtainable p−n homojunctions. Until now, producing a stable p-type ZnO remains a great challenge, and the fabrication of reliable p-type thin films is really a bottleneck, which delays the launching of ZnO-based optoelectronic devices on the market.[4] Zinc oxide exhibits naturally an n-type conductivity that originates from the incorporation of "hidden" hydrogen atoms within the ZnO host lattice to give rise to a large amount of shallow donor levels.[6] The design of a p-type ZnO requires for its part the stabilization of shallow acceptor levels, which should overcompensate the n-donor contribution. While this may be achieved by numerous strategies (Li, P, As doping, for instance[1−4]), the substitution of nitrogen for oxygen appears at first sight as the most appropriate solution in generating hole carriers. This stems from the strong similarity between the two chemical elements in terms of ionic radius and positioning in energy of their 2p-orbitals. In that respect, many synthetic efforts were dedicated to the preparation of N-doped ZnO.[7−12] However, because of the versatility of the electrical behavior reported in the literature for nitrogen-doped or codoped ZnO,[7,9] the p-typeness in these materials is still the subject of controversy.[1−4] This belief has been even accentuated after theoretical investigations, which clearly demonstrate the impossibility to stabilize shallow acceptor levels in Zn-rich ZnO by N-doping only.[13,14] The energy level related to the nitrogen atom on the oxygen site is relatively deep, making acceptor ionization difficult. Alternatively, doping Zn-poor ZnO by nitrogen remains surprisingly an almost unexplored strategy to achieve p-typeness. Although, after Limpijumnong et al.,[15] n-type ZnO might be theoretically converted to p-type ZnO via the injection of Zn vacancies triggered by the substitution of Sb^{5+} for Zn^{2+}, leading to the charge balance $3Zn^{2+} \rightarrow Sb^{5+} + 2V_{Zn} + 1h^{+}$. Such a substitution should occur under oxygen-rich synthesis conditions to hinder the charge self-compensation with formation of oxygen vacancies. On the basis of this reasoning, Allenic et al.[16] succeeded in preparing p-type ZnO:P thin films, the p-typeness being directed by O-rich annealing conditions. The pivotal influence of the atmosphere was also noticed during the preparation of nominally undoped p-type ZnO in which the oxygen pressure was optimized: n-typeness and p-typeness were stabilized under low and high oxygen partial pressure, respectively.[17−20] More recently, Yi et al. also reported the control of p-type conductivity in ZnO:Li films under high oxygen partial pressure

Received: September 9, 2011
Published: November 17, 2011

favoring Zn poor conditions.[21] Prompted by these stimulating results, we have therefore embarked on the quest of p-type ZnO by investigating the nitrogen insertion in Zn-poor ZnO obtained under oxygen-rich conditions with zinc peroxide ZnO_2 as precursor.

EXPERIMENTAL DETAILS

Synthesis. ZnO_2 nanoparticules used as precursor were synthesized according to the chemical route proposed by Uekawa et al.[22,23] Nitrogen-doped ZnO particles were prepared from ZnO_2 by ammonolysis as schemed in Figure 1 of that work. First, 300 mg of ZnO_2 precursor in an alumina boat was placed in a furnace. This one was swept by N_2 for ~10 min to flush out air, before introduction of NH_3 with a controlled 20 L/h flow (Air liquide – purity >99.9%). A plateau at 190 °C for 30 min, as well heating rates of 10 °C/min, were set to limit the projections and dissemination of the product into the furnace when ZnO_2 decomposes (strong exothermic reaction). Synthesis temperatures (T_f) range from 220 to 550 °C. These temperatures were dwelled for 30 min, before the samples were colled to room temperature by turning off the furnace. It is worth noting that the synthetic conditions may severely impact the purity of the samples. In particular, great attention has to be paid to the heating rate, the mass of precursor, and the NH_3 flow rate.

X-ray Powder Diffraction. X-ray powder diffraction patterns were recorded at room temperature in the 10°–80° 2θ range on a Bruker D8 Advance diffractometer using Cu K-L2,3 radiation. All data treatments and refinement were carried out with the JANA2006 package.[24]

Chemical Analysis. Nitrogen and oxygen contents were determined with a LECO TC-600 analyzer using the inert gas fusion method. Nitrogen was detected as N_2 by thermal conductivity and oxygen as CO_2 by infrared detection. The apparatus was calibrated using Leco standard oxides as well as Si_2N_2O as a nitrogen reference. The estimation of the error on the measurement is lower than 5%. The Zn content was obtained by difference. Semiquantitative chemical analyses performed with the use of a scanning electron microscope JEOL 5800 equipped with an energy dispersive X-ray (EDX) microanalyzer were in good agreement with previous estimations.

Spectroscopic Studies. The Raman spectra were collected using a Jobin Yvon T64000 Raman spectrophotometer with an argon ion laser for excitation (λ_{exc} = 514 nm). X-ray photoelectron spectroscopy (XPS, Mg K-L3 = 1253.6 eV) was performed in a Leybold–Heraeus ultrahigh vacuum environment with an analyzer operating in the constant pass energy mode (31.5 eV). Spectra were calibrated in energy using C 1s = 284.7 eV as reference, and the resolution was estimated at about 0.9 eV.

Density Measurements. The AccuPyc 1330 system was used for density measurements by pycnometry under He pressure.

Photoelectrochemical Measurements. Photoelectrochemical measurements were carried out on pressed pellets (sintered at 300 °C under N_2 for 30 min) in a lithium perchlorate electrolyte (0.5 M in water) with a platinum counter electrode and a saturated calomel reference electrode. The spectral photocurrent response was obtained with an AUTOLAB PGSTAT302N (serial no.: AUT83589) under chopped illumination made by an Oriel lamp calibrated to AM 1.5 intensity (1000 W m^{-2}).

Mott–Schottky Measurements. Capacitance measurements were carried out on the same pellets as the ones described previously in a lithium perchlorate electrolyte (0.5 M in water) with a platinum counter electrode and a saturated calomel reference electrode. A potentiostat (potentiostat/galvanostat model VSP from Biologic Sciences Instruments) allows one to plot the capacitance as a function of potential under depletion condition based on the Mott–Schottky relationship $(1)/(C^2) = (2)/(\varepsilon\varepsilon_0 A^2 eN)(V - V_{fb} - (k_B T)/(e))$, where C is the capacitance of the space charge region, ε is the dielectric constant of the semiconductor, ε_0 is the permittivity of free space, N is the charge carrier density (electron donor concentration for an n-type semiconductor or hole acceptor concentration for a p-type semiconductor), V is the applied potential, and V_{fb} is the flatband potential.[25] A negative slope and a positive slope of the C(V) curves are expected for p-type and n-type charge carriers, respectively.

Ultrafast Transient Absorption Measurements. ZnO:N films were prepared by drop casting on glass slides a colloidal solution of 8 months aged ZnO:N nanoparticles prepared at 250 °C in ethanol. The films were then cut into 1 cm wide sections and placed in a saturated acetone solution of the PMI sensitizer. The films were allowed to soak for 12 h prior to measurement, at which point they were washed with acetone and dried with nitrogen. A drop of 0.1 mM LiI/1.0 mM I_2 in propylene carbonate was placed on the sample and covered with a clean 1 cm glass slide. Ultrafast transient absorption measurements were acquired with a previously reported transient absorption system.[26] Excitation of the sample was achieved with ca. 120 fs laser pulses at 510 nm (700 nJ/pulse) through the back contact, enabling the pump and probe to interact with the sensitized film before passing through the surrounding electrolyte. Transient absorption spectra and kinetics are an average of 500 shots per time point. The collected data were binned in 3 nm increments to enhance the signal-to-noise.

RESULTS AND DISCUSSION

Zinc peroxide, ZnO_2, exhibits an interesting pyrite type structure with peroxide $(O_2)^{2-}$ groups. These peroxide groups are very unstable, and their decomposition by firing ZnO_2 at low temperature (210 °C) in air produces wurtzite-type ZnO nanoparticles.[22,23] ZnO_2 appears therefore as an ideal precursor to get a Zn-poor ZnO as the breakdown of the peroxides $(O_2)^{2-}$ groups might favor a large partial pressure of oxygen during the decomposition reaction. With the aim to prepare N-doped Zn-poor ZnO, we have performed a low temperature ammonolysis of zinc peroxide. Figure 1 depicts the temperature profile used to carry out the nitridation of the ZnO_2 nanoparticules under NH_3 atmosphere. All ZnO_2 samples were heated to a final temperature (hereafter labeled T_f) ranging from 220 to 550 °C and maintained at this temperature for 30 min. Samples were then cooled to room temperature by turning off the furnace. All products were subsequently analyzed via the X-ray diffraction technique. Figure 1 demonstrates that they all exhibit X-ray powder patterns consistent with the ZnO-wurtzite structure type with no byproduct detected. The wide diffraction peaks of the X-ray patterns are associated with nanometric particles as asserted by SEM photographs. Moreover, as expected, we note that the higher is the T_f temperature, the higher is the particle size and the smaller is the specific surface area. Hence, going from 220 to 500 °C, the specific surface area (the crystallite size) falls (increases) from 61 to 32 m^2/g (from 13 to 26 nm), respectively. Figure 2 depicts, for all prepared samples, the evolution of the density, the cell volume, and the N, O, and Zn weight percents versus T_f. Clearly, density is constant for T_f between 220 and 300 °C, then strongly increases between 300 and 400 °C, and finally tends asymptotically toward 5.70, the value obtained for "stoichometric" ZnO prepared from ZnO_2 by heating in air at 900 °C for 2 h (hereafter labeled ZnO-ref). In parallel, it is noteworthy that the cell volume exhibits a minimum for T_f around 400 °C. These two observations suggest that T_f strongly impacts the chemical composition of ZnO:N samples. In fact, chemical analyses reveal a large amount of nitrogen for all samples prepared at T_f lower than 320 °C. Above this temperature, the nitrogen concentration approaches zero (or a value lower than the detection threshold of

dx.doi.org/10.1021/ja208044k | J. Am. Chem. Soc. 2012, 134, 464–470

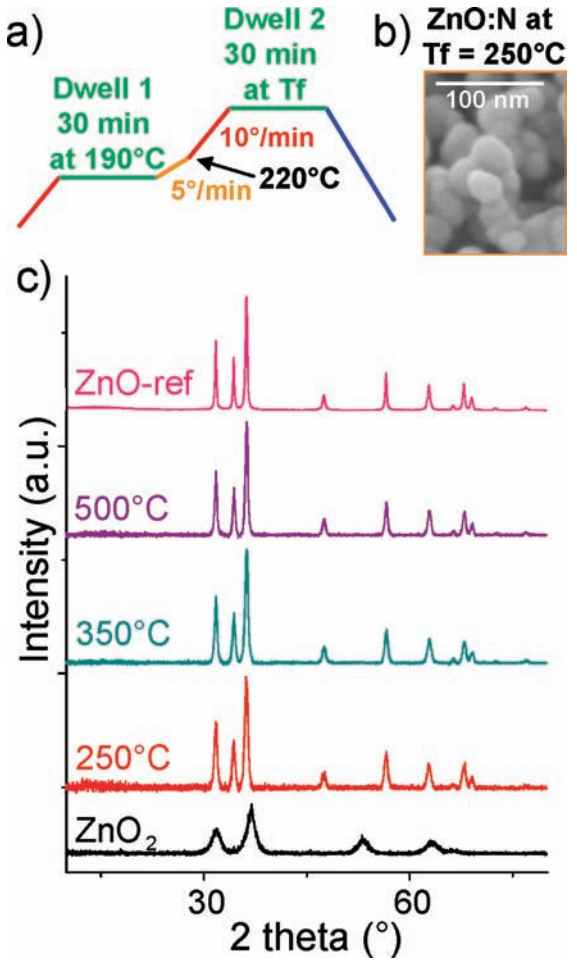

Figure 1. Sample preparation and characterization. (a) Schematic representation of temperature profile used to prepare under NH_3 the materials from the ZnO_2 precursor. (b) Scanning electron microscope picture of the nanometric particles prepared at 250 °C. (c) Powder X-ray diffraction patterns of nitrogen-doped zinc oxide samples prepared at 250, 350, and 500 °C. The patterns of ZnO_2 and of our reference ZnO sample (ZnO-ref) are given for comparison.

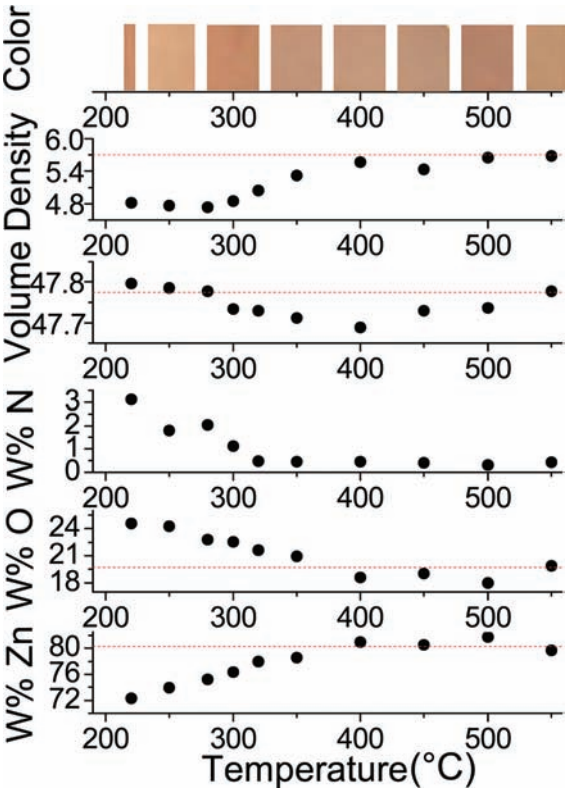

Figure 2. Photographs of synthesized samples, density, refined cell volume (Å^3), and mass percent of O, Zn, and N of prepared ZnO:N samples versus the synthesis temperature T_f. The dotted line indicates the expected values for a "stoichometric" 1:1 zinc oxide.

the technique). Moreover, the examination of the evolution of the Zn and O content in "ZnO" versus the synthesis temperature reveals a striking feature. We observe that the oxygen content decreases and the zinc content increases when T_f shifts from 220 to 400 °C. On the other hand, above 400 °C, the zinc and oxygen weight percents measured for our samples are close to the expected values for stoichometric ZnO. This clearly demonstrates that all samples prepared below 400 °C exhibit a defect of zinc as compared to the 1:1 stoichiometry. Using the measured density, the chemical analysis, and the refined cell volume, we were able to calculate an experimental composition for all of our samples. These results are displayed in Table 1. The chemical composition shifts from $Zn_{0.80(2)}O_{0.97(2)}N_{0.08(2)}$ for Zn-poor N-doped samples to $Zn_{1.00(2)}O_{1.02(2)}N_{0.03(2)}$ for Zn-rich slightly N-doped ones when T_f goes from 220 to 550 °C, respectively. Surprisingly, the chemical composition does not impact severely the ZnO:N material hue because all ammonia treated samples exhibit a similar salmon color (Figure 2). Hence, in addition to the steep absorption threshold at 3.0 eV inherited from undoped ZnO, a second absorption band with an onset at 2.0 eV shows up once nitrogen is inserted (absorption spectra not shown here). The existence of this second absorption band has already been reported for N-containing ZnO samples[10] and is commonly associated with the creation of a midgap state built upon N 2p orbitals.[10,13,16,27] So far, this color is considered as the signature of nitrogen in the host lattice. On the basis of this statement, N-traces would remain in our materials prepared at T_f higher than 320 °C.

To gain more insight into the chemical species present in our ZnO samples, they were examined at room temperature by Raman and X-ray photoelectron spectroscopies. Figure 3a displays the Raman spectra collected using an argon ion laser (λ_{exc}= 514 nm) for N-doped ZnO samples prepared at 250, 350, and 500 °C, and for ZnO_2 and ZnO-ref used as references. Inspection of Raman spectra reveals, in complement with the typical active modes of the ZnO−wurtzite host lattice (i.e., bands peaking at about 330, 383, and 437 cm^{-1}), the absorption bands classically ascribed to the nitrogen-related local vibration modes (i.e., near 275, 507, 583, and 635 cm^{-1}).[27−29] Thus, as well as chemical analyses and absorption spectra, Raman spectroscopy provides strong evidence that nitrogen atoms are incorporated in the ZnO host lattice and substitute at the oxygen site[28] even in compounds synthesized at high temperature (i.e., T_f > 320 °C). Another salient feature of the ZnO:N Raman spectra concerns the absorption peak at about 843 cm^{-1}, which is clearly detectable for samples prepared at temperature lower than 350 °C (Figure 3b). This peak observed in ZnO_2 and already reported for ZnO materials was prepared by firing ZnO_2 in air at 200 °C for 2 h.[23] It has to be regarded as the fingerprint of O−O

dx.doi.org/10.1021/ja208044k |J. Am. Chem. Soc. 2012, 134, 464–470

Table 1. Experimental Chemical Compositions and Proposed Charge Balances of ZnO:N Samples Prepared by Ammonolysis at T_f Temperature[a]

T_f	chemical composition	proposed charge balance
220 °C	$Zn_{0.80}O_{0.97(2)}N_{0.08(2)}$	$(Zn^{2+})_{0.80}(O_2^{2-})_{0.29(1)}(O^{2-})_{0.39(1)}(N^{3-})_{0.08(2)}$
250 °C	$Zn_{0.77}O_{0.97(2)}N_{0.09(2)}$	$(Zn^{2+})_{0.77}(O_2^{2-})_{0.335(10)}(O^{2-})_{0.30(1)}(N^{3-})_{0.09(2)}$
300 °C	$Zn_{0.81}O_{0.98(2)}N_{0.06(2)}$	$(Zn^{2+})_{0.81}(O_2^{2-})_{0.26(1)}(O^{2-})_{0.46(1)}(N^{3-})_{0.06(2)}$
350 °C	$Zn_{0.92}O_{1.00(2)}N_{0.02(2)}$	$(Zn^{2+})_{0.92}(O_2^{2-})_{0.11(1)}(O^{2-})_{0.78(1)}(N^{3-})_{0.02(2)}$
400 °C	$Zn_{0.99}O_{0.93(2)}N_{0.03(2)}$	$(Zn^{2+})_{0.99}(O_2^{2-})_{0.0}(O^{2-})_{0.93(2)}(N^{3-})_{0.03(2)}$
450 °C	$Zn_{0.96}O_{0.93(2)}N_{0.02(2)}$	$(Zn^{2+})_{0.96}(O_2^{2-})_{0.0}(O^{2-})_{0.93(2)}(N^{3-})_{0.02(2)}$
500 °C	$Zn_{0.99}O_{1.03(2)}N_{0.02(2)}$	$(Zn^{2+})_{0.99}(O_2^{2-})_{0.0}(O^{2-})_{1.03(2)}(N^{3-})_{0.02(2)}$
550 °C	$ZnO_{1.02(2)}N_{0.03(2)}$	$(Zn^{2+})_{1.00}(O_2^{2-})_{0.0}(O^{2-})_{1.02(2)}(N^{3-})_{0.03(2)}$

[a] Charge balances for samples prepared at 500 and 550 °C can be achieved only by taking into account the standard deviations on O and N ratios.

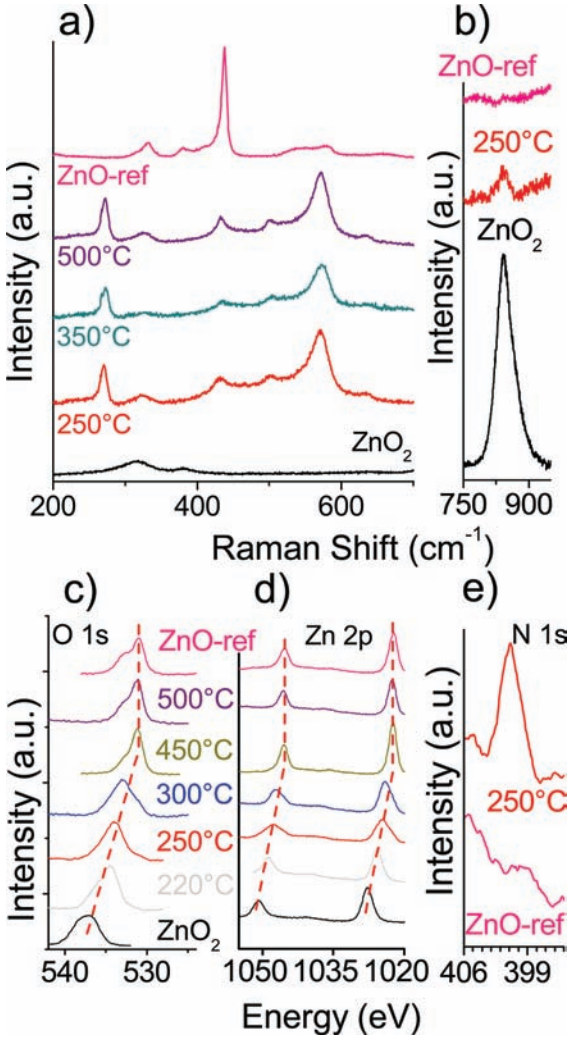

Figure 3. Raman and XPS spectroscopic spectra of ZnO:N samples obtained by ammonolysis of ZnO_2 at T_f. (a) Raman spectra in the 200−800 cm^{-1} range. (b) Raman signature of the presence of O−O pairs in ZnO:N prepared at 250 °C. (c) O 1s XPS spectra of ZnO:N samples (the high energy shoulders are ascribed to −OH surface contamination). (d) Zn 2p XPS of ZnO:N samples. (e) N 1s XPS signature of ZnO:N sample prepared at 250 °C.

peroxide groups in ZnO:N samples prepared at low temperature (see Table 1). For temperature higher than 400 °C, no signature of O−O pairs is detected. This observation goes along with our O 1s XPS analyses (Figure 3c), which evidence within the ZnO:N series a regular shift in energy of this peak with T_f (from 534.0 to 530.9 eV). This variation range matches perfectly the expected energy scale for ZnO_2 (536.8 eV) and ZnO (530.4 eV after[30]). Note also that the shoulder observed on the left of the O 1s peak can be ascribed to OH contamination according to literature data.[31] This suggests that the main surface contamination for this series of compounds is an OH contamination, which is difficult to ride off. To conclude, the overall evolution of the O 1s peak in energy may be viewed as the signature of peroxide groups maintained in materials synthesized at low temperature. Oxo O^{2-} and peroxo $(O_2)^{2-}$ ions coexist up to 350 °C with a progressive disappearance of O−O pairs with temperature. Beyond, O−O pairs are thermodynamically too unstable to be stabilized anymore in the wurtzite structure. Similar conclusions may be drawn from the examination of the XPS Zn $2p_{3/2}$ and $2p_{1/2}$ states (Figure 3d). Again, for ZnO:N samples prepared below 350 °C, these states exhibit intermediate binding energy between those found in ZnO-ref and ZnO_2. This strongly supports the occurrence of Zn^{2+} cations homogeneously surrounded by oxo and peroxo groups with a $O^{2-}/(O_2)^{2-}$ ratio depending on the synthesis conditions. Finally, Figure 3e displays the N 1s XPS spectra of ZnO:N synthesized at T_f = 250 °C with ZnO-ref. Clearly, the N 1s binding energy (BE) of 399.7 eV is close to the BE observed for N^{3-} anions in oxynitrides.[32,33] However, on the basis of these XPS measurements, the occurrence of N−N or N−O bonds cannot be totally excluded because these species can exhibit N 1s BE located in 402.5−403.7 eV[33] and 401−405 eV[34] energy domains, respectively. Further investigations are clearly needed to clarify the oxidation state of nitrogen and to raise the ambiguity concerning the possible occurrence of N−N or N−O bonds. It is well beyond the scope of the present study to fully address the nitrogen oxidation state assignment in these ZnO:N compounds, which is a very complex issue as illustrated by the recent deep debates in the similar case of nitrogen-doped TiO_2 compounds.[34,35] To sum up, both XPS and Raman spectroscopic studies suggest the presence of Zn^{2+}, O^{2-}, $(O_2)^{2-}$, and nitrogen anionic species (under an undetermined form) in our samples with ratios depending on the synthesis temperature, T_f. The peroxide groups are stabilized at temperature lower than ~350 °C, and the nitrogen content falls below 320 °C. Interestingly, the presence of peroxide groups is also required to account for the charge balances of the low temperature phases whatever the oxidation state considered for nitrogen. According to the determined chemical formulations (see Table 1), the

dx.doi.org/10.1021/ja208044k | J. Am. Chem. Soc. 2012, 134, 464–470

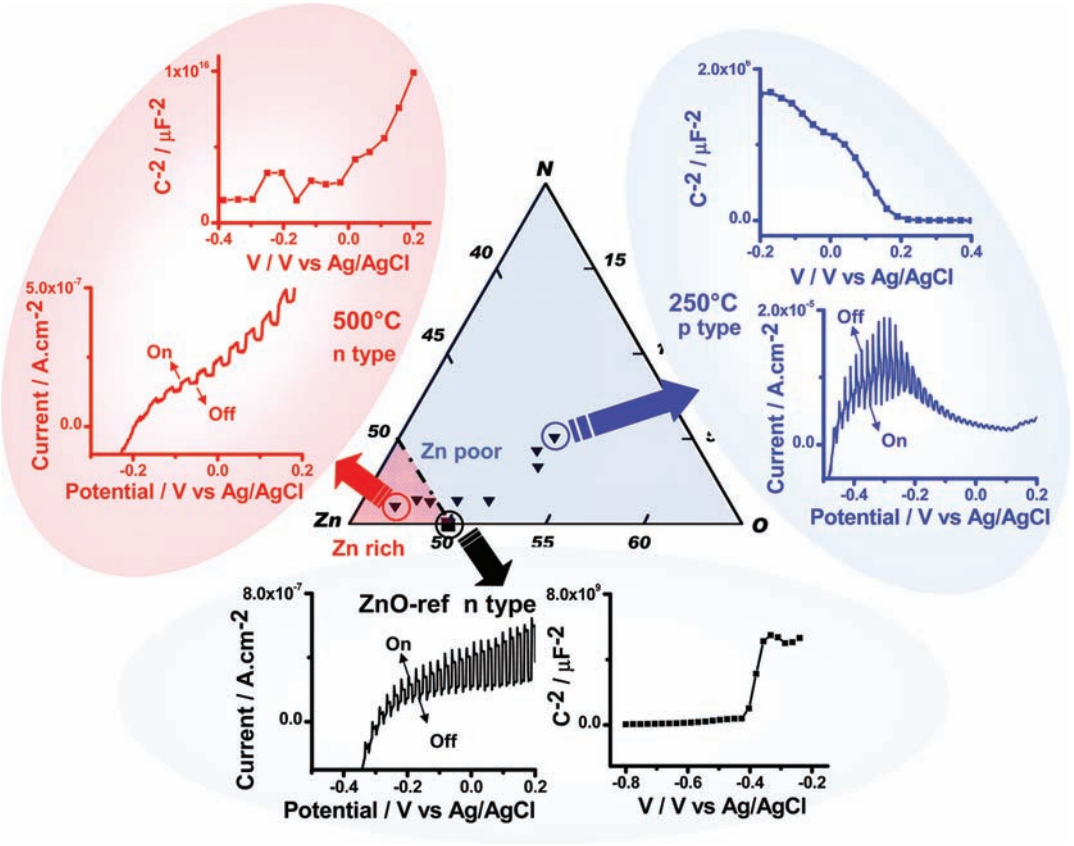

Figure 4. Electrochemical (Mott−Schottky) and photoelectrochemical caracterization of ZnO:N prepared at 250 °C (blue ellipse), 550 °C (red ellipse), and ZnO-ref (gray ellipse). The comparison with the ternary phase diagram reporting the compositions of all compounds suggests that ZnO poor nitrogen-doped samples are p-type while Zn-rich samples are n-type (on = under illumination, off = in the dark).

charge balance assuming Zn^{2+} and O^{2-} cannot be satisfied whatever the oxidation state of the nitrogen anionic species. Charge balance can be achieved only if $(O_2)^{2-}$ groups are taken into account. Thus, for instance, the chemical composition calculated for the sample prepared at 220 °C would be $Zn^{2+}_{0.80(2)}([O_2]^{2-})_{0.29(1)}(O^{2-})_{0.39(1)}N^{3-}_{0.08(2)}$ considering N^{3-} or $Zn^{2+}_{0.80(2)}([O_2]^{2-})_{0.25(1)}(O^{2-})_{0.47(1)}N^{2-}_{0.08(2)}$ considering N^{2-}. Table 1 reports hypothetical chemical compositions calculated assuming arbitrarily the presence of N^{3-}. It shows that in low temperature prepared compounds, almost 60% of the oxygen atoms would be present as peroxide groups in this case. Alternatively, no O_2 dimers have to be invoked in compounds prepared at high temperature (T_f > 350 °C) to reach the right charge balance.

To check the influence of the presence of Zn vacancies on the carrier type in our ZnO:N samples, we have first performed room temperature Hall measurements on pressed pellets. These pellets were annealed in mild conditions (350 °C for 30 min) under nitrogen gas to prevent alteration of the carrier type and to favor the cohesion between grains. Unfortunately, the as-prepared samples were too resistive (10^7−10^8 Ω) to provide reliable results. Thus, photoelectrochemical studies were undertaken.[36] This technique was successfully used recently to examine the charge carrier type of nanoparticles of well-known p-type semiconductors $CuGaO_2$ and LaOCuS.[37−39] Figure 4 displays the current−potential curves under chopped illumination of pellets of ZnO-ref and ZnO:N samples synthesized at 250 and 500 °C. Pellets were prepared in the aforementioned conditions. For ZnO:N prepared at 250 °C, the $I(V)$ curve evidenced a drop in intensity under illumination associated with a strong increase of the reductive component of the current, giving rise to small negative oscillations whose amplitude is enhanced as potentials become more negative. This phenomenon originates from the higher relative increase in the negative charge carriers as compared to the positive charge carriers in the material when photoexcited. This is a clear signature of the p-typeness of the ZnO:N sample. Conversely, ZnO-ref and materials prepared at 500 °C (or above 350 °C) display an expected behavior for n-type semiconductors, which show an increase in the current under illumination. At this stage, it is worth noting here that nitrogen-free Zn-poor ZnO samples prepared from decomposition in air of ZnO_2 at 250 °C do not show a p-type conductivity, while they exhibit a similar amount of Zn vacancies as compounds prepared under NH_3 flow. Our experiments demonstrate that only a combination of Zn vacancies with nitrogen doping gives rise to the stabilization of p-type conductivity. Interestingly, the current−potential curve of the p-type ZnO:N sample prepared at 250 °C was measured regularly over a period of 2 years. All measurements attest that the p-type character of this compound is retained during this period when stored in air under ambient conditions. Moreover, the inverse square capacitance value of the space charge region obtained at different applied potentials was also examined and compared between the three samples (Figure 4). Again, it is observed that a 2 year old ZnO:N powder prepared at 250 °C displayed p-type semiconductor characteristics as asserted by

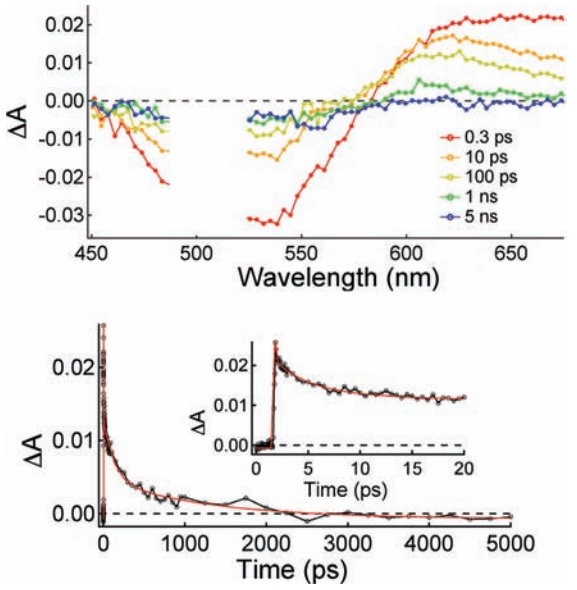

Figure 5. Ultrafast transient absorption measurements. (a) Transient absorption spectra of PMI/ZnO excitation at 510 nm of PMI/ZnO at various time delays: 0.3 ps (red), 10 ps (orange), 100 ps (yellow), 1 ns (green), and 5 ns (blue). (b) Kinetics trace: kinetic data at 650 nm after 510 nm excitation, along with the best fit line. The inset shows the same kinetic data on the 20 ps time scale.

the negative slope of the $C^{2-}(V)$ curve. On going from ZnO-ref and the n-type ZnO:N sample prepared at 500 °C to the p-type ZnO:N sample prepared at 250 °C, the sign of the slope on the Mott−Schottky plot change from positive to negative, highlighting the intricate relationship between the synthetic conditions and the final electrical behavior. Moreover, the Mott−Schottky plots reveal that the flatband potential (intercept of the line with potential abscise) increases by more than +0.8 eV in the p-type sample as compared to the reference. This strong change ascertains the shift of the Fermi level toward the conduction band maximum that is expected at the transition from n-type to p-type samples.

Another clear proof of the p-type stability of the 250 °C prepared ZnO:N nanoparticles is provided by ultrafast transient absorption measurements. ZnO:N films sensitized by perylene-monoimid (PMI) were prepared from 8 months aged nanoparticles stored in air. Excitation of the sensitized ZnO:N films results in the formation of excited PMI, which rapidly undergoes hole injection into the mineral, 1.1 ± 0.2 ps. Figure 5a shows the time-resolved spectra of PMI/ZnO, after 510 nm excitation. The spectral features are indicative of laser pulse-limited generation of excited *PMI (broad absorption around 660 nm and ground-state bleach) followed by the formation of the radical anion of the PMI sensitizer (narrower absorption band around 610 nm). Hole injection of PMI has been previously reported for the well-known p-type semiconductor, NiO.[26] The strong similarities between the data presented here and the previous report of PMI sensitized NiO support the p-type character of the ZnO material. Recombination of the PMI^-/ZnO^+ charge separated state occurs over hundreds of picoseconds and is best fit with two time constants, 14 ± 2.6 and 460 ± 33 ps, as shown in Figure 5b. Despite rapid recombination, the hole injection process is readily observed and is indicative of the p-type nature of the ZnO:N nanoparticles.

CONCLUSION

The exothermic transformation of ZnO_2 into ZnO at temperature lower than 350 °C under ammonia engenders a Zn-poor zinc oxide with a wurtzite structure type in which the O^{2-}, $(O_2)^{2-}$ species coexist with nitrogen anionic species. The combination of a high zinc vacancy concentration with insertion of nitrogen and coexistence of oxide and peroxide groups can lead to the stabilization of positive charge carriers. Consequently, a perfect control of the synthetic conditions is necessary to access p-typeness (temperature in particular). Once achieved, the p-type character of these nanoparticles is stable over more than 2 years. This spectacular stability should permit their use in numerous applications and will likely open the way to various applications of ZnO-based optoelectronics.

ASSOCIATED CONTENT

Supporting Information. Complete ref 21. This material is available free of charge via the Internet at http://pubs.acs.org.

AUTHOR INFORMATION

Corresponding Author
laurent.cario@cnrs-imn.fr; stephane.jobic@cnrs-imn.fr

ACKNOWLEDGMENT

This project was part of the PERLE and NANOFONC programs financed by Région Pays de la Loire. A.S. and L.H. are thankful for support from the K&A Wallenberg Foundation and The Swedish Research Council. Vincent Fernandez and Jean-Yves Mevellec are thanked for their help in XPS and Raman studies, respectively.

REFERENCES

(1) Özgür, Ü.; Alivov, Y. I.; Liu, C.; Teke, A.; Reshchikov, M. A.; Doan, S.; Avrutin, V.; Cho, S. J.; Morkoc, H. *J. Appl. Phys.* **2005**, *98*, 041301.
(2) Pearton, S. J.; N., D. P.; Ip, K.; Heo, Y. W.; Steiner, T. *Prog. Mater. Sci.* **2005**, *50*, 293–340.
(3) Look, D. *Mater. Sci. Eng., B* **2001**, *80*, 383–387.
(4) Look, D. C.; Claflin, B. *Phys. Status Solidi B* **2004**, *241*, 624–630.
(5) Huang, M. H.; Mao, S.; Feick, H.; Yan, H.; Wu, Y.; Kind, H.; Weber, E.; Russo, R.; Yang, P. *Science* **2001**, *292*, 1897–1899.
(6) Van de Walle, C. G. *Phys. Rev. Lett.* **2000**, *85*, 1012–1015.
(7) Cao, P.; Zhao, D. X.; Zhang, J. Y.; Shen, D. Z.; Lu, Y. M.; Yao, B.; Li, B. H.; Bai, Y.; Fan, X. W. *Appl. Surf. Sci.* **2008**, *254*, 2900–2904.
(8) Minegishi, K.; Koiwai, Y.; Kikuchi, Y.; Yano, K.; Kasuga, M.; Shimizu, A. *Jpn. J. Appl. Phys.* **1997**, *36*, L1453–L1455.
(9) Li, J.; Kykyneshi, R.; Tate, J.; Sleight, A. W. *Solid State Sci.* **2007**, *9*, 613–618.
(10) Mapa, M.; Gopinath, C. S. *Chem. Mater.* **2009**, *21*, 351–359.
(11) Sato, Y.; Sato, S. *Thin Solid Films* **1996**, *281*, 445–448.
(12) Zou, C. W.; Chen, R. Q.; Gao, W. *Solid State Commun.* **2009**.
(13) Lyons, J. L.; Janotti, A.; Van de Walle, C. G. *Appl. Phys. Lett.* **2009**, *95*, 252105.
(14) Zhang, S. B.; Wei, S. H.; Zunger, A. *J. Appl. Phys.* **1998**, *83*, 3192–3196.
(15) Limpijumnong, S.; Zhang, S. B.; Wei, S. H.; Park, C. H. *Phys. Rev. Lett.* **2004**, *92*, 155504.
(16) Allenic, A.; Guo, W.; Chen, Y. B.; Katz, M. B.; Zhao, G. Y.; Che, Y.; Hu, Z. D.; Liu, B.; Zhang, S. B.; Pan, X. Q. *Adv. Mater.* **2007**, *19*, 3333–3337.

(17) Ma, Y.; Du, G. T.; Yang, S. R.; Li, Z. T.; Zhao, B. J.; Yang, X. T.; Yang, T. P.; Zhang, Y. T.; Liu, D. L. *J. Appl. Phys.* **2004**, *95*, 6268–6272.
(18) Oh, M. S.; Kim, S. H.; Seong, T. Y. *Appl. Phys. Lett.* **2005**, *87*, 122103.
(19) Xiong, G.; Wilkinson, J.; Mischuck, B.; Tüzemen, S.; Ucer, K. B.; Williams, R. T. *Appl. Phys. Lett.* **2002**, *80*, 1195.
(20) Zeng, Y. J.; Ye, Z. Z.; Xu, W. Z.; Lu, J. G.; He, H. P.; Zhu, L. P.; Zhao, B. H.; Che, Y.; Zhang, S. B. *Appl. Phys. Lett.* **2006**, *88*, 262103.
(21) Yi, J. B.; et al. *J. Phys. Rev. Lett.* **2010**, *104*, 137201.
(22) Uekawa, N.; Kajiwara, J.; Mochizuki, N.; Kakegawa, K.; Sasaki, Y. *Chem. Lett.* **2001**, *30*, 606–607.
(23) Uekawa, N.; Mochizuki, N.; Kajiwara, J.; Mori, F.; Wu, Y. J.; Kakegawa, K. *Phys. Chem. Chem. Phys.* **2003**, *5*, 929–934.
(24) Petricek, V.; Dusek, M.; Palatinus, L. *JANA 2006: The Crystallographic Computing System*; Institute of Physics: Praha, Czech Republic, 2006.
(25) Sato, N. *Electrochemistry at Metal and Semiconductor Electrodes*; Elsevier: Amsterdam, 1998.
(26) Morandeira, A.; Boschloo, G.; Hagfeldt, A.; Hammarström, L. *J. Phys. Chem. B* **2005**, *109*, 19403–19410.
(27) Uekawa, N.; Mitani, Y.; Kojima, T.; Kakegawa, K. *Nippon Seramikkusu Kyokai Gakujutsu Ronbunshi* **2009**, *117*, 283–288.
(28) Kaschner, A.; Haboeck, U.; Strassburg, M.; Kaczmarczyk, G.; Hoffmann, A.; Thomsen, C.; Zeuner, A.; Alves, H. R.; Hofmann, D. M. *Appl. Phys. Lett.* **2002**, *80*, 1909–1911.
(29) Kerr, L. L.; Li, X.; Canepa, M.; Sommer, A. J. *Thin Solid Films* **2007**, *515*, 5282–5286.
(30) Moulder, J. F.; Stickle, W. F.; Sobol, P. E.; Bomben, K. D.; D., K. *Handbook of X-Ray Photoelectron Spectroscopy*; Perkin-Elmer: Eden Prairie, MN, 1995.
(31) Lee, Y.; Shimodaira, H. T. Y.; Teramura, K.; Hara, M.; Kobayashi, H.; Domen, K.; Yashima, M. *J. Phys. Chem. C* **2007** **2007**, *111*, 1042–1048.
(32) Kamath, A.; Kwong, D. L.; Sun, Y. M.; Blass, P. M.; Whaley, S.; White, J. M. *Appl. Phys. Lett.* **1997**, *70*, 63–65.
(33) Le Gendre, L.; Marchand, R.; Laurent, Y. *J. Eur. Ceram. Soc.* **1997**, *17*, 1813–1818.
(34) Gopinath, C. S. *J. Phys. Chem. B* **2006**, *110*, 7079–7080.
(35) Burda, C.; Gole, J. *J. Phys. Chem. B* **2006**, *110*, 7081–7082.
(36) Schiavello, M. *Photochemistry, Photocatalysis and Photoreactors: Fundamentals and Developments*; Reidel: Dordrecht, 1985.
(37) Doussier-Brochard, C.; C., B.; Cario, L.; Jobic, S. *Inorg. Chem.* **2010**, *49*, 3074–3076.
(38) Srinivasan, R.; Chavillon, B.; Doussier-Brochard, C.; Cario, L.; Paris, M.; Gautron, E.; Deniard, P.; Odobel, F.; Jobic, S. *J. Mater. Chem.* **2008**, *18*, 5647–5653.
(39) Chavillon, B.; Cario, L.; Doussier-Brochard, C.; Srinivasan, R.; Le Pleux, L.; Pellegrin, Y.; Blart, E.; Odobel, F.; Jobic, S. *Phys. Status Solidi A* **2010**, *207*, 1642–1646.